2A.5 ENHANCED DUAL-WAVELENGTH TECHNIQUE FOR REMOTE DETECTION OF CLOUD LIQUID WATER CONTENT

John K. Williams*, J. Vivekanandan and Guifu Zhang
National Center for Atmospheric Research, Boulder, Colorado

1. INTRODUCTION

Reliable remote detection of cloud liquid water content (LWC) and droplet sizes is important both for understanding cloud microphysics and meteorological processes and for providing improved diagnostics of icing potential for the aviation community. One particularly promising technique makes use of the ratio of reflectivities measured by co-located millimeter radars operating at different wavelengths, such as K_a and W-bands or X and K_a-bands. This dual-wavelength ratio (DWR) may be used to obtain signal attenuation and thereby infer the liquid water density along the radar beams. Unfortunately, useful implementation of the DWR technique has been hindered by its sensitivity to reflectivity measurement error, Mie scattering, and artifacts due to mismatched radar beam sizes and radar locations. The retrieval of reasonable LWC values often requires significant averaging, which seriously degrades the resolution and accuracy of the retrievals.

The present paper elucidates the mechanisms responsible for contaminating the DWR retrievals, describes censoring and smoothing techniques for mitigating this contamination, and presents a method for boosting the resolution of the smoothed values to nearly that of the raw reflectivity measurements. Results obtained using K_a and W-band data from the Mount Washington Icing Sensor Project (MWISP) field program illustrate the performance of this enhanced DWR retrieval technique.

2. DUAL-WAVELENGTH TECHNIQUE

The dual-wavelength method for retrieving liquid water content profiles is based on the observation that liquid water attenuates radar signals differently depending on their wavelengths (Doviak and Zrnić, 1993; Vivekanandan, et al., 1999 and 2001). Under "small-droplet" conditions, the attenuation of radar measurements at wavelength λ is given by

$$\frac{\partial}{\partial r}\left(dBZ(r) - dBZ_{\lambda}(r)\right) = L(r)\,a_L(\lambda,r) + a_G(\lambda,r), \qquad (1)$$

where $dBZ(r)$ is the true reflectivity at range r along the radar beam, $dBZ_{\lambda}(r)$ is the reflectivity attenuated by the two-way attenuation of the intervening medium, $L(r)$ is the liquid water content (g/m^3), $a_L(\lambda,r)$ is the liquid attenuation coefficient (dB/km/(g/m^3)), and $a_G(\lambda,r)$ is the gas attenuation coefficient (dB/km).

* *Corresponding author address:* John K. Williams, National Center for Atmospheric Research, P.O. Box 3000, Boulder, CO 80307; email: jkwillia@ucar.edu.

Substituting two distinct wavelengths into equation (1), subtracting the equations, and rearranging yields

$$L(r)\left[a_L(\lambda_2,r) - a_L(\lambda_1,r)\right] = \frac{\partial}{\partial r}\left(dBZ_{\lambda_1}(r) - dBZ_{\lambda_2}(r)\right) - \left[a_G(\lambda_2,r) - a_G(\lambda_1,r)\right]. \qquad (2)$$

Equation (2) states that, when adjusted for gas attenuation, the range derivative of the radar-measured reflectivity difference is proportional to the liquid water content, the constant of proportionality being the differential liquid attenuation of the two wavelengths. This equation, which relates the unknown liquid water content to the measured reflectivities, is the basis of the dual-wavelength technique.

Once a reliable liquid water profile has been computed and $dBZ(r)$ has been estimated by integrating equation (1), a useful estimate of particle diameter, called radar estimated size (RES), may be obtained from

$$\mathrm{RES(r)} = \left(\frac{\langle D^6(r)\rangle}{\langle D^3(r)\rangle}\right)^{1/3} = \left(\frac{\pi\rho_w}{6}\frac{Z(r)}{L(r)}\right)^{1/3} \qquad (3)$$

(Vivekanandan, et al., 2001), where $\langle D^n(r)\rangle$ denotes the n^{th} moment of the droplet size distribution at range r and ρ_w is the density of water.

3. SOURCES OF ERROR

In applying equation (2) in practice, several sources of error affect the accuracy of the retrieved liquid water content values. These include errors in the values of the liquid and gas attenuation coefficients; errors in the measured reflectivities caused by Mie scattering, mismatches of the radars' measurement volumes ("geometric" error); noise in the radar measurements; and errors due to the computation of the range derivative using the discrete range gates at which measurements are available. Inserting terms for each of these errors and using "hats" for estimated quantities, equation (2) becomes

$$\left[\hat{A}_L(\lambda_1,\lambda_2,r) - E_{A_L}(r)\right]L(r) = \hat{A}_L(\lambda_1,\lambda_2,r)\hat{L}(r) - \hat{D}_r\left(E_{noise}(r)\right) - E_{\hat{D}_r}(r) - \frac{\partial}{\partial r}\left(E_{Mie}(r) + E_{geom}(r)\right) + E_{A_G}(\lambda_1,\lambda_2,r) \qquad (4)$$

Here $\hat{A}_L(\lambda_1,\lambda_2,r) = \hat{a}_L(\lambda_2,r) - \hat{a}_L(\lambda_1,r)$ is the estimated differential liquid attenuation coefficient; $E_{A_L}(r) = \hat{A}_L(\lambda_1,\lambda_2,r) - \left[a_L(\lambda_2,r) - a_L(\lambda_1,r)\right]$; $\hat{A}_G(\lambda_1,\lambda_2,r) = \hat{a}_G(\lambda_2,r) - \hat{a}_G(\lambda_1,r)$ signifies the estimated differential gas attenuation coefficient; $E_{A_G}(r) = \hat{A}_G(\lambda_1,\lambda_2,r) - \left[a_G(\lambda_2,r) - a_G(\lambda_1,r)\right]$; $\hat{D}_r$ denotes a

discrete derivative operator (e.g., a finite difference), assumed to be linear; $E_{D_r}(r) = \hat{D}_r\left(dBZ_{\lambda_1}(r) - dBZ_{\lambda_2}(r)\right) - \frac{\partial}{\partial r}\left(dBZ_{\lambda_1}(r) - dBZ_{\lambda_2}(r)\right)$; $\hat{Z}_\lambda(r)$ represents the radar-measured reflectivity for wavelength λ at range r; E_{Mie}, E_{geom}, and E_{noise} represent errors in the dual-wavelength ratio due to Mie scattering, geometric mismatch errors, and measurement noise, respectively; and $\hat{L}(r)$ is defined by $\hat{A}_L(\lambda_1,\lambda_2,r)\hat{L}(r) = \hat{D}_r\left(d\hat{BZ}_{\lambda_1}(r) - d\hat{BZ}_{\lambda_2}(r)\right) - \hat{A}_G(\lambda_1,\lambda_2,r)$. The discrete derivative of the measurement noise, the discrete differentiation operator error, the derivative of the Mie scattering and geometric mismatch errors, and the differential gas attenuation error each cause an error in the liquid water content estimate proportional to the true differential liquid attenuation coefficient, $\hat{A}_L + E_{A_L}$, while the error in the differential liquid attenuation coefficient produces a relative error. These various sources of errors and methods for mitigating them are discussed below.

3.1 Differential attenuation factors

Errors in the values of the attenuation coefficients a_L and a_G may be due to either inappropriateness of the formulas used to compute them or to uncertainties in the temperature, pressure, and relative humidity values needed to compute them. For example, Figure 1 shows a plot of differential liquid water attenuation coefficient vs. temperature for two radar wavelength pairs. Uncertainty in temperature over the domain –20 to 0°C may cause a relative error of at most 3.7% in $a_L(\lambda_2,r) - a_L(\lambda_1,r)$ for the K_a- and W-band pair, but as much as 67% for the X- and K_a-band pair. This miscalculation propagates directly into the value of the liquid water content estimate, yielding a bias of magnitude $\frac{E_{A_L}(\lambda_1,\lambda_2,r)}{a_L(\lambda_2,r) - a_L(\lambda_1,r)}\hat{L}(r)$. Similarly, uncertainty in the value of temperature, pressure, or humidity creates an error in the differential gas attenuation coefficient and generates a bias equal to $\frac{E_{A_G}(\lambda_1,\lambda_2,r)}{a_L(\lambda_2,r) - a_L(\lambda_1,r)}$ in the retrieved LWC. For the K_a- and W-band pair, for instance, this error could be as high as 0.049 g/m^3 for temperatures between –20 and 0°C, pressure between 500 and 1000 mb, and humidity between 0 and 100%.

The magnitude of the errors caused by uncertainties in the differential attenuation coefficients should be one of the factors considered when designing a dual-wavelength system. In addition, an operational DWR algorithm should include checks to make sure that conditions satisfy the requirements for the attenuation coefficients' computations, and should assess the error generated by uncertainties in the temperature, pressure, and relative humidity profiles.

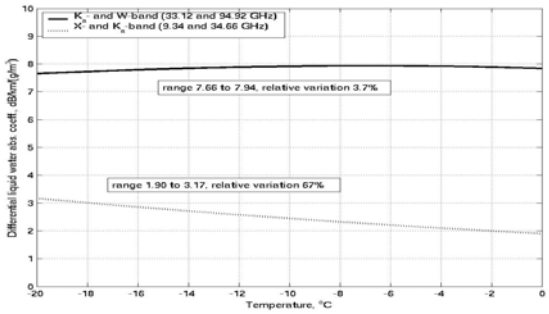

Figure 1: Dependence of the differential liquid water attenuation coefficient, $a_L(\lambda_2,r) - a_L(\lambda_1,r)$, on temperature for K_a and W-band (top) and X and K_a-band (bottom) radar pairs.

3.2 Geometric mismatch

Because a radar inherently averages reflectivity over an illumination volume, an error may be introduced when the (attenuated) reflectivity is non-linear over that volume, in which case the illumination-averaged reflectivity does not match the value at the pulse volume center. When two radars have illumination volumes of substantially different sizes, the error in the DWR caused by this effect can be considerable. Similarly, if the radars are displaced so that they are sampling different regions of the atmosphere, any inhomogeneity in reflectivity could cause large errors in the DWR.

Consider, for example, the two situations depicted in Figure 2, where one radar beam detects the moving cloudlet before the other. As the concentration of liquid water passes into the first beam, both the reflectivity and the attenuation of the radar signal increase in the ranges of intersection, while those of the second beam remain small. Therefore, the DWR, $d\hat{BZ}_{\lambda_2}(r) - d\hat{BZ}_{\lambda_2}(r)$, becomes large for the ranges containing the liquid water. As a result, the DWR's range derivative is positive at the near side of this region and negative at the far side, with a slight negative trend in between due to attenuation; this causes the retrieved LWC for the near ranges to have a strong positive bias, while giving the LWC of the far ranges experiences a negative bias. Averaging the retrieved LWC over time and range may provide some mitigation of this contamination, at the cost of reducing the resolution of the retrieval.

The paired over- and under-estimate artifacts caused by beam mismatch appear very similar to those caused by two other effects: range sampling mismatches or Mie scattering. The first of these occurs when the range gates of the two wavelengths are slightly displaced, or the range gate spacing is different for the two, requiring one profile to be interpolated onto the grid for the other. For example, the CPRS K_a- and W-band radars used in MWISP employed range-gate spacings of 75 m and 30 m, respectively; they were interpolated onto a common 30 m grid to facilitate

comparison. The displacement or smoothing of sharp reflectivity features often causes matched over- and under-estimates in the DWR. On the other hand, Mie scattering occurs when large droplets (diameters $> \lambda_2/16$) reduce the backscatter for the radar having the smaller wavelength, λ_2, thereby decreasing its measured reflectivity and increasing the DWR within the affected area. Isolated regions of large droplets therefore cause matched positive and negative biases to the retrieved LWC at their near and far ranges, respectively. This effect can be produced by ice or mixed-phase regions as well.

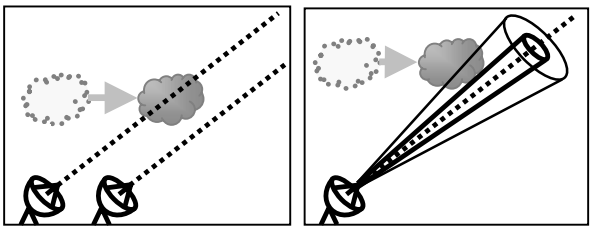

Figure 2: Schematic diagrams of a "cloudlet" advecting past two radars with parallel beams but displaced (left) or having different beam widths (right). Preferential detection of the water by one radar in either case creates an error in the dual-wavelength LWC retrieval.

3.3 Discrete differentiation

Because radars measure reflectivity only at discrete range gates, a discrete differentiation operator is required to estimate the range derivative of the DWR. The central finite difference

$$\hat{D}_r(f(r)) = \frac{f(r+\Delta r) - f(r-\Delta r)}{2\Delta r} \tag{5}$$

is an example of one such operator; it produces an error

$$E_{\hat{D}_r}(r) = \frac{1}{6}(\Delta r)^2 \frac{\partial^3}{\partial r^3} f(r) + \frac{1}{120}(\Delta r)^4 \frac{\partial^5}{\partial r^5} f(r) + \ldots \tag{6}$$

which is minimized when the range gate spacing, Δr, is as small as possible. Unfortunately, such a choice increases the impact of random noise in the DWR values. Indeed, if the random errors $\tilde{f}$ are independent and identically distributed with mean 0, then $\mathrm{var}\left[\hat{D}_r(\tilde{f}(r))\right] = 2\,\mathrm{var}\left[\tilde{f}\right] / (\Delta r)^2$; thus, the random error in the LWC retrieval is inversely proportional to Δr. This noise/resolution tradeoff is the central paradox that limits the accuracy of the dual-wavelength technique.

4. ENHANCED TECHNIQUE

The first step of the new technique is to perform smoothing of the measured DWR to reduce the effect of random noise and the artifacts described above. This may be done in two steps: first, the raw data are used assign "confidence" weights to each value of the DWR, and then the smoothed values are computed using trimmed-mean, confidence-weighted kernel filtering. Confidences are assigned based on the SNR estimated from the measured reflectivities (values near or below zero are assigned low confidence), and the linear depolarization ratio (LDR) coupled with the measured reflectivities (high values of LDR or reflectivity indicate ice or large droplets and hence Mie scattering conditions, and yield low confidence). For each DWR point, a Gaussian kernel is used to weight near values more than distant ones, and the final weights are generated as the product of the Gaussian values and the confidence weights. Finally, the confidence-weighted trimmed mean of the DWR values is computed by removing a percentage of the highest and lowest values (according to their weights) and then computing the weighted mean value of those remaining. This computation balances the advantages of weighted median and trimmed mean filtering, and effectively interpolates through regions of bad data. Finally, the liquid and gas attenuation coefficients are computed using temperature, pressure, and relative humidity from a proximate sounding or other estimate, and the DWR method is applied to obtain an LWC estimate, $\bar{L}$.

To "boost" the smoothed LWC values into higher-resolution retrievals, the new technique exploits the observation made by Frisch, et al. (1998) that the ratio of $L/Z^{1/2}$ is more stable than either reflectivity or LWC themselves. In fact, Frisch's method for retrieving LWC assumes that this ratio is constant for the entire profile, and computes it based on the radiometer-measured total liquid path and radar-measured reflectivities. With the availability of the low-resolution LWC from the DWR method, a local $L/Z^{1/2}$ ratio can be computed, and this quantity may then be used along with the measured reflectivities to obtain a high-resolution LWC estimate, $\hat{L}$. For the results shown in the next section, the $L/Z^{1/2}$ ratio at each range gate, r, was found by computing a best-fit line of the form $\bar{L} = \kappa \hat{Z}^{1/2}$ using the LWC and reflectivity values from a temporal and spatial region around the point; the new LWC was computed via $\hat{L}(r) = \kappa(r)\hat{Z}(r)^{1/2}$. The reflectivity field was then adjusted to remove the effect of attenuation caused by the estimated LWC, and the process was iterated until a stable value of $\hat{L}$ was determined.

5. RESULTS

The method described above was applied to the UMASS CPRS K_a-, and W-band radar data obtained in MWISP between 16:20 and 16:40 UTC on April 14, 1999. This case was selected because the NOAA X- and K_a-band radars, CPRS K_a- and W-band radars, and NOAA radiometer were all operating and were directed at a common elevation angle of about 18.5°. In addition, the K_a-band linear depolarization ratios suggest that very little ice or mixed-phase was present, except for the last few minutes of this period. The application of the new technique to the NOAA X- and

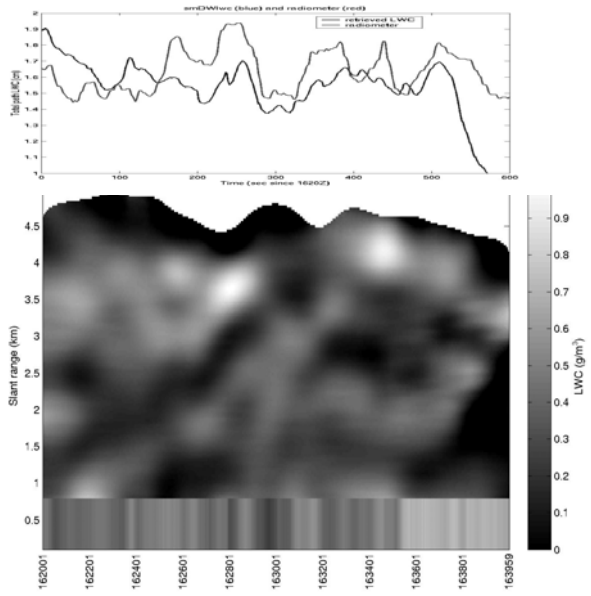

Figure 3: (Bottom) Timeseries of smoothed LWC profiles retrieved from the DWR of the CPRS K_a- and W-band radar data collected between 1620 and 1640 Z on April 14, 1999 using the method described in the text for slant ranges 0 to 5 km. The initial range gates were filled in using the first good DWR values at about 0.8 km. LWC values range from 0 g/m^3 (black) to 1 g/m^3 (white) as indicated by the colorbar to the right. (Top) Timeseries of total-path liquid water from the retrieved LWC (black) and the collocated NOAA radiometer (gray). The y-axis ranges from 1.0 to 2.0 mm.

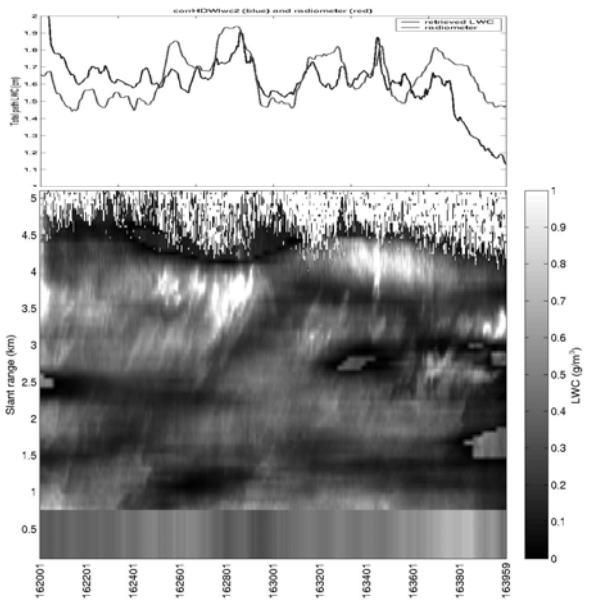

Figure 4: Same as Figure 3 but showing the results of the high-resolution retrieval technique described in the text.

K_a-band data was also attempted, but the very weak gradient in the DWR made any LWC retrieval difficult.

The gray-scaled plot in Figure 3 shows a timeseries of LWC profiles obtained from smoothing the CPRS K_a- and W-band DWR as described above and then applying the DWR method. A comparison of the integrated LWC to the radiometer liquid path is also shown. The poor correlation at the beginning and end of the time interval may be partly due to the fact that a full smoothing window was not available there; the underestimate at the end is likely due to a region of Mie scattering. Nevertheless, these values show reasonable correlation, even though the smoothness of the retrieved LWC field does not appear realistic.

Figure 4 shows a similar plot, but with the W-band reflectivity values used to "boost" the resolution using the new technique described above. The correlation of the integrated LWC with the radiometer-measured value appears at least as good as for the smoothed case, and the resolution of the LWC field is improved.

6. CONCLUSION

The technique presented in this paper shows promise in reducing the impact of several phenomena that corrupt the measured DWR, offering a new method for retrieving high-resolution, range-resolved LWC profiles using dual-wavelength radar data. Further work remains to be done in refining and verifying the technique, however. Refinements may include the use of image processing techniques to explicitly identify and remove artifacts caused by geometric errors, and adaptive smoothing regions based on the quality of the data. Verification should involve both simulation using realistic cloud models and further application to field program data with coordinated in-situ measurements available for comparison.

7. ACKNOWLEDGEMENT

This research is in response to requirements and funding by the Federal Aviation Administration (FAA). The views expressed are those of the authors and do not necessarily represent the official policy or position of the FAA.

6. REFERENCES

Doviak, R. J., and Zrnić, D. S., 1993: *Doppler Radar and Weather Observations*. Academic Press, 562 pp.

Frisch, A. S., Feingold, G., Fairall, C. W., Uttal, T., and Snider, J. B., 1998: On cloud radar and microwave radiometer measurements of stratus cloud liquid water profiles. *J. Geophys. Res.*, 103, D18, 23,195–23,197.

Vivekanandan, J., Martner, B. E., Politovich, M. K., and Zhang, G., 1999: Retrieval of atmospheric liquid and ice characteristics using dual-wavelength radar observations. *IEEE Trans. on Geosci. Remote Sens.*, 37, 2325–2334.

Vivekanandan, J., Zhang, G., and Politovich, M. K., 2001: An assessment of droplet size and liquid water content derived from dual-wavelength radar measurements on the application of aircraft icing detection. *J. Atm. and Oceanic Tech.*, 18, 1787–1798.